

1 **Early maturation** processes in coal.

2 Part 1: Pyrolysis mass balances and structural evolution of coalified wood from the  
3 Morwell Brown Coal seam

4  
5 Elodie Salmon <sup>a,c</sup>, Françoise Behar <sup>a</sup>, François Lorant <sup>a</sup>, Patrick G. Hatcher <sup>b</sup>, Paul-Marie  
6 Marquaire <sup>c</sup>.

7 *a Institut Français du Pétrole, BP 311, 92506 Rueil-Malmaison cedex, France*

8 *b Department of Chemistry and Biochemistry, Old Dominion University, Norfolk, VA,*  
9 *USA 23529*

10 *c Département de Chimie Physique des Réactions, Institut Polytechnique de Lorraine, 1*  
11 *rue Grandville, B.P.20451 F, 54001 Nancy cedex, France.*

12  
13 Corresponding author:

14 François Lorant, IFP (Institut Français du Pétrole), Département de Géochimie, 1 et 4 avenue  
15 du bois Préau, 92852 Rueil-Malmaison, France, tel : 33 14 752 6910 fax : 33 14 752 7019,  
16 email : francois.lorant@ifp.fr  
17

18

19  
20  
21  
22  
23  
24  
25  
26  
27  
28  
29  
30  
31  
32  
33  
34  
35

## Abstract

In this work, we develop a theoretical approach to evaluate maturation process of kerogen-like material, involving molecular dynamic reactive modeling with a reactive force field to simulate the thermal stress. The Morwell coal has been selected to study the thermal evolution of terrestrial organic matter. To achieve this, a structural model is first constructed based on models from the literature and analytical characterization of our samples by modern 1-and 2-D NMR, FTIR, and elemental analysis. Then, artificial maturation of the Morwell coal is performed at low conversions in order to obtain, quantitative and qualitative, detailed evidences of structural evolution of the kerogen upon maturation. **The observed chemical changes are a defunctionalization of the carboxyl, carbonyl and methoxy functional groups coupling with an increase of cross linking in the residual mature kerogen. Gaseous and liquids hydrocarbons, essentially CH<sub>4</sub>, C<sub>4</sub>H<sub>8</sub> and C<sub>14+</sub> liquid hydrocarbons, are generated in low amount, merely by cleavage of the lignin side chain.**

Keywords: thermal decomposition, Morwell coal, molecular model, coal maturation, lignite.

## 36 1. **Introduction:**

37 Thermal stress in the Earth's subsurface is one of the most important forces driving  
38 hydrocarbon generation from kerogen in shales and coal (Philippi, 1965; Louis **and** Tissot,  
39 1967; Albrecht and Ourisson, 1969). For terrestrial material that typically forms coal, the  
40 main **hydrocarbon** is methane gas. However, in some cases, coal is considered to be a source  
41 of paraffinic-rich hydrocarbons of **molecular weight higher** than methane or volatile  
42 hydrocarbon gases (Mukhopadhyay et al., 1991; Fowler et al., 1991, Nelson et al., 1998). Of  
43 particular interest in this current study is the origin of methane and other gaseous  
44 hydrocarbons, especially from precursor chemical structures like lignin. Previous studies have  
45 shown that lignin is an important precursor for coal structures (Hatcher, 1989) and that  
46 methane is generated in abundance as the main hydrocarbon from such a structural  
47 component of wood during maturation (Behar and Hatcher, 1995). Moreover, here are many  
48 kerogens whose organic matter is partly sourced from terrestrially-derived organic matter  
49 which contains as its main constituent lignin. Knowing the hydrocarbon-generating potential  
50 and mechanism from the lignaceous components of such kerogens is **of paramount interest**  
51 to assessing the relative importance of terrestrial organic matter in the overall hydrocarbon  
52 potential of these kerogens (**Behar and Hatcher, 1995**).

53 The work reported in the present paper is part of a study that aims at establishing, from  
54 a theoretical point of view, the primary cracking mechanism for **insoluble sedimentary**  
55 **organic matter** derived exclusively from lignin. This paper addresses the structural study of  
56 specific **insoluble sedimentary organic matter** materials and the construction of the  
57 corresponding molecular models. We also describe the thermal decomposition, at low  
58 conversions, of a sample in which we deduce the initial chemical reactions for conversion.  
59 For this purpose, a lignitic wood from the Morwell coal (Victorian brown coal, Australia) was  
60 selected as our precursor material, recognizing that it has already undergone some maturation

61 to achieve a coal rank of lignite (**Hatcher, 1988**). This wood sample has previously been  
62 shown by flash pyrolysis/gas chromatography/mass spectrometry to contain mainly lignin-  
63 derived structures (Behar and Hatcher, 1995). In a previous study, the chemical structural  
64 composition and a proposed structural model for gymnospermous wood was presented  
65 (Hatcher, 1989). However, a model for angiospermous lignite has yet to be proposed.

66 Our approach is to first compare our chemical analyses to chemical models previously  
67 proposed in the literature for similar samples. Based on both literature models and our own  
68 analyses, updated chemical structures are proposed for a material derived from  
69 angiospermous wood. Closed pyrolysis of the wood in gold tubes followed by a detailed  
70 quantitative analysis of the products, including the matured lignite residue, allows for mass  
71 balances of products and determination of the overall transformation processes during  
72 simulated maturation. Thermal decomposition products are identified using numerous  
73 techniques such as elemental analyses, gas chromatography (GC) coupled to flame ionization  
74 detection (FID) or thermal conductivity detection (TCD), infrared (IR) spectroscopy, and  
75 solid and liquid state  $^{13}\text{C}$  NMR.

76

## 77 **2. Sample: Lignite from the Morwell coal**

78 **The Morwell lignite was collected from the Morwell Open Cut, Latrobe Valley,**  
79 **Victoria, Australia and is composed essentially of angiospermous wood transformed to**  
80 **the rank of lignite B (Hatcher, 1988; Behar and Hatcher, 1995).** It is part of an entire  
81 fossil tree buried at the peat stage in the Early Miocene and coalified within the deposit.  
82 During early diagenesis, biodegradation and mild chemical processes led to the  
83 decomposition of the cellulose and the hemi-cellulose and transformed the lignin structure  
84 into lignite (Spackman and Barghoorn, 1966; Philp et al., 1982; Stout et al., 1988; Hatcher et  
85 al., 1989, Hatcher and Clifford, 1997). The sample was freeze-dried and ground to a fine

86 powder with a mortar and pestle and stored under nitrogen gas. **This sample is ideal for this**  
87 **study because it is naturally organic rich, no chemical treatment is needed to extract the**  
88 **organic matter and it is thermally immature.**

89

### 90 **3. Experimental**

91 The experimental procedures used in this study have been described in detail by  
92 Salmon et al. (**accepted manuscript**). In this previous work, similar experiments were  
93 performed on an aliphatic biopolymer, algaenan from *Botryococcus braunii* race L. The  
94 structural evolution of the Morwell lignite was performed by characterizing the initial sample  
95 and the recovered residues from simulated maturations at various temperatures and times.  
96 Elemental analysis (combustion/pyrolysis in a Carlo-Erba system) is used to quantify the  
97 proportions of C, H and O. Chemical functional groups are measured by Attenuated Total  
98 Reflectance Fourier Transform Infrared (ATR – FTIR) spectroscopy on a Bruker Tenser 27  
99 spectrometer.

100 Detailed structural characterizations are obtained by direct polarisation and magic angle  
101 spinning (DPMAS)  $^{13}\text{C}$  NMR and High Resolution Magic Angle Spinning (HRMAS) NMR  
102 techniques on a Bruker AVANCE II Ultra Shield <sup>TM</sup> 400 MHz spectrometer. Solid-state  $^{13}\text{C}$ -  
103 NMR spectra were obtained using the basic direct polarization pulse program as described  
104 previously (Dria et al., 2002). Approximately 80 mg of sample was inserted into an NMR  
105 rotor and spun at the magic angle ( $54.7^\circ$ ) with a frequency of 15 kHz. A 45 degree pulse angle  
106 and a 10 s recycle time were used for each of 10,000 accumulations. Exactly 1024 data points  
107 were collected on the free induction decay and an exponential line broadening of 100 Hz was  
108 applied prior to Fourier transformation. The spectra were integrated by dropping vertical lines  
109 to the baseline between chemical shift regions characteristic of the various types of functional  
110 groups.

111 HRMAS spectroscopy was performed with the same NMR spectrometer as described  
112 above using a CHN z-axis gradient HRMAS probe. Approximately 20 mg of sample was  
113 swelled in DMSO-d<sub>6</sub> (Aldrich, 99.9 atom % D) as it was packed into a 4 mm diameter  
114 zirconia MAS rotor spun at the magic angle at 9 kHz. A relaxation delay of 1 s was used for  
115 each experiment. A <sup>1</sup>H-<sup>13</sup>C heteronuclear single quantum coherence (HSQC) spectrum was  
116 acquired using echo-antiecho gradient selection. In the <sup>1</sup>H dimension (F2), 344 scans were  
117 acquired, each collected with 1024 data points for a spectral width of 4,006 Hz (10.01 ppm).  
118 In the <sup>13</sup>C dimension (F1), 128 data points were collected for a spectral width of 166 ppm.  
119 Line broadening was used in both dimensions, 1 Hz in the F1 and 0.3 Hz in the F2 dimension.  
120 The FIDs were processed in both dimensions using a squared sine multiplication (QSINE)  
121 window function.

122 A total correlation spectroscopy (TOCSY) spectrum was acquired with a phase  
123 sensitive pulse program that used States-TPPI and the MLEV-17 multiple pulse spin lock  
124 sequence. A mixing time of 60 ms was used. A spectral width of 6000 Hz (15 ppm) was  
125 obtained in both dimensions. In the F2 dimension, 128 scans were acquired, with 2048 data  
126 points. In the F1 dimension, 256 data points were collected and zero-filled to 512. The FIDs  
127 were processed in the F2 dimensions using a -3 Hz Gaussian line broadening and in the F1  
128 dimension using a line broadening of 1.0 and a QSINE window function. All of the HRMAS  
129 spectra obtained on the 400 MHz spectrometer were calibrated using the DMSO peak,  
130 referenced to tetramethylsilane (TMS) at 0 ppm.

131 Artificial maturation was performed in gold tube reactors according to methods  
132 described by Al Darouich et al. (2006). **Constant temperature confined pyrolysis is**  
133 **performed at 200, 225, 250, 275 and 300°C during 9h.** Two tubes were used for each  
134 temperature/time condition, one for gaseous product analysis and the other for liquid product  
135 analysis. Gas analysis was performed on one gold tube pierced in a vacuum line equipped

136 with a Toepler pump (Behar et al., 1989). Gas chromatography using a thermal conductivity  
137 detector was used to characterise and quantify of all the individual gases generated. Two  
138 liquid fractions were extracted : the first one recovered the hydrocarbons and the lightest  
139 NSOs compounds by pentane extraction, the second one was a dichloromethane extraction for  
140 the recovery of most of the heavy hydrocarbons and heteroatom-containing hydrocarbons.  
141 Extraction was performed by stirring under reflux for 1 hour. An initial aliquot of the pentane  
142 extract was used for quantification of the C<sub>6</sub>-C<sub>14</sub> compounds. This aliquot was fractionated on  
143 a micro column of silica gel into saturated and aromatic compounds. An internal standard (C<sub>25</sub>  
144 *n*-alkane) was added for the quantification by GC-FID. The *n*-C<sub>5</sub> compounds were not  
145 quantified because pentane is used as solvent. The second aliquot was evaporated and  
146 quantified. A second extraction was performed with dichloromethane (DCM) by stirring  
147 under reflux for 1 hour. The DCM extract was evaporated and quantified by weighing. The  
148 insoluble residue of this extraction was then dried and weighed. Mass and atomic balances  
149 were done in order to check the recovery yield of all the pyrolysis products.

150

## 151 **4. Results and discussions**

### 152 *4.1. Initial structure*

153 To our knowledge, no molecular model of the Morwell lignite has been proposed to  
154 date in the literature. However a molecular model (Figure 1) of an Australian brown coal (or  
155 lignite B) from the Yallourn Open Cut (near the Morwell Open Cut, Holgate, 1985) was  
156 proposed by Hatcher (1989) from the experimental data of Bates and Hatcher (1989) and  
157 using as a structural motif the lignin model of fresh gymnosperm wood proposed by Alder  
158 (1977). This Adler model was transformed by applying experimental observations of  
159 peatification and early coalification reactions (Hatcher and Clifford, 1997).

160 We compared the atomic and structural compositions of this gymnosperm coal model  
161 with experimental data (elemental and solid-state  $^{13}\text{C}$  NMR) obtained on the Morwell lignite  
162 (Behar and Hatcher, 1995) that is summarized in Table 1. Results show that, except for the  
163 amount of carboxylic groups, the distribution of oxygenated functional groups of the Morwell  
164 lignite is very similar to that of the gymnosperm coal model. The major difference is the  
165 relative proportion of aliphatic and aromatic carbons. The Morwell lignite is enriched in  
166 aliphatic carbon. The Morwell lignite, however, is an angiospermous wood as determined by  
167 the flash pyrolysis data shown in Behar and Hatcher (1995). In fact, angiospermous wood  
168 contains syringyl based units not found in gymnospermous wood (Philp et al., 1982).  
169 Therefore, use of the gymnospermous coal model of Hatcher (1989) is inappropriate to  
170 describe the structural nature of the Morwell lignite sample. Hence, we develop a new  
171 structural model for Morwell lignite that uses the same approach used by Hatcher (1989) but  
172 is derived from the angiospermous lignin structural motif of Nimz (1974) and is constrained  
173 by the new experimental data obtained in the current study (elemental analysis, FTIR, and  
174 NMR) along with reactions that have been proposed in previous studies (e.g., demethylation,  
175 removal of oxygen functional groups from side-chains, aryl ether cleavage-see Hatcher and  
176 Clifford, 1997).

177 Reactions of peatification and early coalification have been determined from  
178 observations of structural compositions of fresh wood samples and lignitic samples (Stout et  
179 al., 1988, Hatcher et al., 1989, Hatcher, 1989, Behar and Hatcher, 1995, McKinney and  
180 Hatcher, 1996). Figure 2 summarizes reactions we feel are important in transforming the  
181 carbon skeleton of the Nimz lignin model. In order to constrain reaction sites, distances  
182 between the reactant functional groups are computed from the coordinates of the individual  
183 atoms modeled in 3-D space as described below. Reactions are assumed to occur if the  
184 distances are below a distance of three single C-C bonds. Hence the lignin model shown in

185 Figure 3 is constructed to represent the likely structure of the Morwell lignite built around the  
186 Nimz motif. We use Cerius<sup>2</sup> (version 4.8.1, Accerlys software) and minimized our structure  
187 with the UFF\_VALBOND 1.1 force field (a combination of the original VALBOND method  
188 described by Root et al., 1993, augmented with non-orthogonal strength functions taken from  
189 Root, 1997 and the Universal Force Field of Rappé et al., 1992) to produce atomic  
190 coordinates.

191 With the reactions shown in Figure 2, the carbon skeleton of the Nimz model is  
192 rearranged, furan-like structures are removed and the proportion of side-chain hydroxyl/ether  
193 groups decreases significantly. Then the proportion of each functional groups are readjusted  
194 in the structure to match with quantitative NMR data (Table 2) and better represent the  
195 structure of coalified angiospermous wood that is equivalent in rank to the Morwell lignite .  
196 Thus, eleven hydroxyl functions are oxidized to carboxyl groups (reaction 6) and two are  
197 reduced to yield unsubstituted aliphatic carbons (reaction 7). Twenty methoxy functions are  
198 demethylated to yield hydroxyl aryl functions (reaction 8). Dehydroxylation of two hydroxyl  
199 aryl groups (reaction 9) allow for the adjustment of the proportions of aryl-O groups. The  
200 structural model thusly obtained for the Morwell coal is displayed in Figure 4. This model  
201 now serves as the basis for further reactions deduced from artificial maturation in sealed gold  
202 tubes. We modify this model in accordance with the chemical analyses of the residue and the  
203 liquid and gaseous products.

204

#### 205 *4.2. Observed chemical changes during thermal decomposition of Morwell lignite*

206 As mass balances given in Table 3 show, the total mass loss of the Morwell coal was  
207 16.64% at 300 °C exposed for 9 h. The elemental composition changes significantly as  
208 demonstrated by the atomic composition of the recovered lignite that exhibits a precipitous  
209 decrease of both H/C and O/C ratios with values down to 0.69 and 0.22, respectively.

210 Concurrently, CO<sub>2</sub> is generated at temperatures starting as low as 200 °C, reaching a  
211 maximum yield of 12.99 wt% at the most severe conditions and representing 3.6% of the  
212 carbon balance. This value is similar to the combined carbon loss from the carboxyl (2.9%)  
213 and carbonyl (0.6%) functions as estimated by NMR (Figure 5).

#### 214 4.2.1. Structural evolution observed by DPMAS NMR.

215 We calculate the carbon loss from NMR spectra in Figure 5 by multiplying area  
216 percentages for the various integration regions by the total residual carbon from the carbon  
217 mass balance that is based on a starting carbon content of 100 mg. Hence, in the structure,  
218 17% of the carbonyl functions and 44% of the carboxylic groups are decomposed at 300 °C/9  
219 h. The loss of methoxy groups (seen clearly in the NMR spectra of Figure 5) accounts for loss  
220 of 5.3% of carbons, but only 0.11 wt% of methane was recovered in gaseous pyrolysis  
221 products at the temperature of 300 °C. This lack of correspondence between loss of methoxy  
222 groups and methane generation suggests that almost all methoxy species lost are not  
223 converted into methane gas. There are multiple possibilities for the formation of end-  
224 products: one is that the methyl radical formed reacts with other components of the solid  
225 residue, another is reaction of the methyl radical with liquid or volatile products, another is  
226 reaction of the methyl radical with OH radical or water to form methanol which is difficult to  
227 measure by GC/MS and not included in the mass balance. Considering the uncertainty with  
228 which we understand the redistribution of the methyl group, we cannot specifically account  
229 for its fate at the moment, but we can suggest that methane is not the only end-product.

230 We cannot exclude the fact that part or the entire yield of the methane originates from  
231 pyrolytic degradation of aliphatic carbons in the Morwell coal. Butane, produced in higher  
232 yields than methane, is also likely to originate from pyrolytic degradation of aliphatic carbons  
233 in the Morwell coal. In fact, we calculate that a combined 2.76 wt% of methane and butane  
234 are produced, with no contributions from other volatile hydrocarbon gases. The NMR data

235 shows that 8.22% of aliphatic carbons (CH, CH<sub>2</sub>, and CH<sub>3</sub> not including O-substituted  
236 aliphatic groups) are lost from the structure of the Morwell coal heated to 300 °C, more than  
237 enough to account for the volatile hydrocarbons produced, including methane, if one assumes  
238 that aliphatic side chains are the source of these volatile species.

239 If we include O-substituted aliphatic groups and carboxyl/carbonyl species in our  
240 carbon balance, there is a substantial loss of lignin side-chain carbons in the Morwell coal  
241 considering that the initial sample contained 29% C of total carbons associated with such side  
242 chains and the residue contains only 16%. Thus, the carbon skeleton released half of its  
243 aliphatic side chains by defunctionalisation and/or depolymerisation and/or pyrolytic  
244 degradation.

245 Interestingly, the total amount of aromatic carbons ( $fa = \text{aroC} + \text{aryl-O carbons}$ ) increased by  
246 2% (from 64.9% to 66.9% of the carbon). The uncertainty of the peak area in solid-state NMR  
247 is estimated to 3% corresponding to a range of uncertainty for the total aromatic carbon of  
248 more or less 2%. This suggests that no significant amount of aromatic units is released from  
249 the initial structure upon thermal stress. Behar and Hatcher (1995) show that C<sub>6+</sub> pyrolyzate,  
250 extract from residue obtained between 200 and 300°C, is essentially composed of aromatics  
251 structures (benzene, phenol, catechol, guaiacol, syringol and naphthalene were identified).  
252 Thus, if such structures are formed, they should be recovered in the C<sub>6+</sub> pyrolyzate. In fact,  
253 we measure during the experiment at 300°C during 9h, as low as 0.90wt % of C<sub>6+</sub> pyrolyzate.  
254 Using the atomic composition of the extracts (pentane and DCM C<sub>14+</sub> extract) we can estimate  
255 that 0.69% of aromatic carbons are lost which is not significant compared to the uncertainty in  
256 area measurements of 2%. This confirms that the amount of aromatic carbon, in the residue  
257 recovered at 300°C, is similar to the amount in the initial sample. However, the NMR spectra  
258 in Figure 5 show significant changes to the aromatic region. The aryl-O disappears during  
259 artificial maturation and the amount that disappears (6.5% of the total carbon) is not exactly

260 equivalent to the amount of aromatic carbon that appears (8.6%) suggesting that aryl-O  
261 carbons are transformed to aromatic carbons not bearing an O and that additional aliphatics  
262 carbons are converted to aromatic carbons. The proportion of aryl-O functions initially  
263 represents 39.8% of total aromatic carbons (*fa*) and these decreases to 28.8% in the recovered  
264 residue at 300 °C. Hence, we calculate that 6.55% of carbons correspond to 25% of the aryl  
265 functions that are converted into aromatic carbons by losing an oxygen substituent. Two  
266 processes may explain the conversion of the aryl-O carbons to aromatic carbons: Behar and  
267 Hatcher (1995) demonstrated that two dihydroxyle rings link by an ether group is  
268 decomposed to one dihydroxyle units and one monohydroxyle units, another process is that  
269 the aryl functions lose an hydroxyl group like by reaction 9.

270         Considering that the total loses of aryl function is decomposed by deshydroxylation of  
271 aryl-OH functions forming water and that lost of hydroxyl groups in the lignin side chain  
272 generated water, the maximum of carbon involving in dehydration of the mature sample is  
273 estimated to 8.2% C (6.5 % of aryl-O carbons + 1.7% of alkoxy carbons) during artificial  
274 maturation.

#### 275         4.2.2. *Structural evolution observed by FTIR spectroscopy*

276         In agreement with the solid state NMR, the infrared spectra Figure 6 show a sharp  
277 decrease of the C=O and C-O bands relative to the defunctionalisation of the side chain. Only  
278 vibration bands of the aromatic skeletons and of OH are observed in the spectra at 300°C.  
279 Because of conversion of aryl-O carbons to aromatic carbon, noticed by quantitative NMR,  
280 bi- (guaiacol units) and trihydroxyl (synringol) rings are converted in bi- (guaiacol) and  
281 monohydroxyl (p-hydroxyphenol) rings suggested for instance in Hatcher et al. (1989).  
282 Asymmetric deformation bands at 1470 cm<sup>-1</sup> of the aromatic skeleton are replaced by  
283 symmetric deformation bands at 1370 cm<sup>-1</sup>, in the infrared spectra. This change in vibration

284 band is in agreement with the conversion of the syringol and guaiacol asymmetric units into  
285 symmetric units of p-hydroxyphenol.

#### 286 4.2.3. *Structural evolution observed by HRMAS NMR*

287 The HRMAS data shown in Figure 7 and 8 for both the unreacted Morwell coal and  
288 the residue at 300 C/9h provide additional clues as to the specific transformations that occur  
289 during artificial maturation, except for the aromatic region. In the aromatic region of the  
290 HSQC spectra (Figure 7 and 8) the cross peaks for both the untreated and matured samples  
291 are dispersed over a wide chemical shift range and it is almost impossible to assign any one  
292 cross peak to a specific structure. It is apparent that the number of cross peaks diminishes  
293 with increasing maturation, and this may be due to the fact that aromatic rings are becoming  
294 deprotonated as the result of heating. Once deprotonated the cross peaks for aromatic carbons  
295 disappear. On the DPMAS spectra, depicted as a projection on the ordinate, the amount of  
296 aromatic carbon protonated represent a small amount of the total area ascribed to aromatic  
297 carbons. It is important to underline that those small amount do not represent the precise  
298 amount of aromatic carbons protonated but the minimum of those protonated carbons detected  
299 by HSQC NMR.

300 In HRMAS spectra quaternary carbons, such as ketone and carboxyl carbons, are not  
301 detected, thus only the aldehyde, hydroxyl and methoxy oxygenated functional groups are  
302 observed (Figure 7). Aldehyde functional groups, identified as 1, are observed in both  
303 TOCSY spectra (Figure 9) of the untreated and the mature sample which show that aldehydes  
304 persist upon thermal decomposition at 300 °C. However those aldehydes are not be present in  
305 large amounts, because no signal is detected in the region of the carbonyl groups in the HSQC  
306 spectra despite the fact that around 3% are quantified by solid state NMR in the initial coal  
307 and the residue recovered at 300°C. This suggests that carbonyl groups are mainly ketones  
308 which do not show signals in HSQC or TOCSY spectra.

309 In standard lignin structural units, the hydroxyl functions may be substituted in the  $\alpha$ ,  
310  $\beta$  or  $\gamma$  positions of the aliphatic side chain (see Figure 1b). Though, in the initial structure only  
311 hydroxyl functions in the  $\gamma$  position are observed (cross peak 5 in Figure 7, and 8). We cannot  
312 exclude the fact that,  $\alpha$  and  $\beta$  hydroxyl functions fall below the detection threshold. In fact,  
313 0.4% of hydroxyl functions are quantified in the DPMAS spectrum of the recovered residue  
314 whereas in the 2D spectra (HSQC and TOCSY) no signal is observed for these structures. As  
315 observed in quantitative NMR spectrum, the intensity of methoxy functional groups assigned  
316 to signal 6 is significantly decreased compared to the original coal sample.

317 Aliphatic carbons (Figure 8) are assigned to regions 7, 8, 9 corresponding to  $-\text{CH}-$ ,  $-\text{CH}_2-$  and  $-\text{CH}_3$ . In region 7, additional signals (7B, 7C) appear in the residue recovered at  
318  $300^\circ\text{C}$  and signal 7A, ascribed to  $-\text{CH}-$  in benzylic positions, is detected in both the initial  
319 sample and the heated residue. The increase of aliphatic  $-\text{CH}-$  groups in the heated residue is  
320 probably associated with increased cross linking of the aliphatic side chains. In region 8 of the  
321 unheated sample, cross peaks are dispersed and of low intensity, whereas, in the mature  
322 sample, cross peaks are well defined, more intense, and less abundant. This is consistent with  
323 a process involving defunctionalisation of the aliphatic side chains, a process described  
324 previously for the early coalification process (Hatcher and Clifford, 1997; Solomon et al.,  
325 1988). In the unheated sample containing mainly lignin structural units, aliphatic carbons ( $-\text{CH}-$ ,  $-\text{CH}_2-$  and  $-\text{CH}_3$ ) are typically adjacent to carbons substituted by carboxyl, carbonyl and  
326 hydroxyl groups. This can explain why their chemical shifts are broadly dispersed in the  
327 spectrum. Upon thermal stress, oxygenated functional groups are released, leading to an  
328 increasing signal strength for aliphatic carbons and to more uniform structural characteristics  
329 which translate to fewer peaks. Similarly, the TOCSY spectrum (Figure 9 and 10) of the  
330 unheated sample contains more dispersed aliphatic cross peaks than the heated sample  
331 confirming that aliphatic carbons are less diverse in structural makeup following the artificial

334 maturation. Cross peak 8A is assigned to benzylic CH<sub>2</sub> on the aliphatic side chains and  
335 carbons 8B and 8C are attributed to CH<sub>2</sub> groups that are β or γ to the aromatic carbons. The  
336 <sup>1</sup>H chemical shifts of peaks in region 8B are more downfield than the <sup>1</sup>H chemical shifts of  
337 peaks 8C suggesting that 8B structures are more proximal to aromatic rings or to oxygenated  
338 functions than are 8C structures. Increased heating leads to a shift in peaks of region 8B to  
339 lower <sup>1</sup>H chemical shift values. Defunctionalisation of the side chain is probably responsible  
340 for this change. The transformation of structures associated with 8D (unheated sample) to 8D'  
341 (heated sample) is attributed to a rearrangement of the side chain carbons to form a 7-member  
342 alicyclic structure as shown in Figure 8, structure V. The broadening of cross peak 8D' is  
343 consistent with the presence of the naphthenic structures linked to aromatic rings as shown in  
344 Figure 8, structures IX and X. The aromatic naphthenes are also consistent with the evolution  
345 of vibrations bands in the infrared spectrum of the heated sample (see discussion above). An  
346 increased abundance of methyl groups (region 9) is observed in the spectra of the residue  
347 recovered at 300°C. Signals associated with box 9A' correspond to methyl groups in terminal  
348 positions on the propyl or ethyl side chains. Peaks in box 9B are assigned to methyl groups in  
349 benzylic positions, an indication that part of the original aliphatic lignin side chains has been  
350 cleaved.

351 The TOCSY spectra are shown in Figures 9 and 10 and a table of spectral assignments  
352 is also given in Figure 10 for protons in the aliphatic region. The information obtained from  
353 these spectra is entirely consistent with what is observed in the HSQC spectra; except that a  
354 peak is observed for aldehyde protons (1') in the heated coal (Figure 9). This is due to the  
355 higher sensitivity of the TOCSY than the HSQC method. In the aromatic region (Figure 9),  
356 <sup>1</sup>H-<sup>1</sup>H couplings decrease because the amount of protonated aromatic carbons decreases in the  
357 structure (see discussion of HSQC NMR data above). In the aliphatic region (Figure 10), only  
358 CH<sub>3</sub>-CH<sub>2</sub> and CH<sub>2</sub>-CH<sub>2</sub> couplings are detected in both spectra. The absence of peaks J<sub>B</sub> and

359  $J_D$  in the spectrum of the initial sample shows that the amount of coupling through two and  
360 three bonds is very low. This confirms that CH, CH<sub>2</sub> and CH<sub>3</sub> are widely dispersed in the  
361 structure and that carbons substituted by oxygenated functional groups disrupt long range  
362 connectivity within a single spin system. The cross peak  $J_H$ , appearing only in the thermally  
363 stressed sample, is assigned to ethyl side chains on aromatic rings which is in agreement with  
364 the DPMAS NMR data showing that pyrolytic degradation of the aliphatic side chains occurs  
365 during thermal stress.

366

## 367 5. Overall processes of maturations

368 **The changes in molecular-level composition are globally quantified by elemental**  
369 **analysis and solid state NMR, providing constraints for the chemical transformation of**  
370 **the lignin model to the rank of lignite. In addition to gaseous and liquids products**  
371 **derived from artificial maturation, structural evolution of the coalified wood model is**  
372 **described. The carbon balance and thermal decomposition processes are summarized in**  
373 **Figure 11. Pyrolysis experiments, performed at 300°C over a period of 9h, convert**  
374 **10.6% of the Morwell coal carbon into gaseous and liquid products. Early**  
375 **transformations involve mainly the rearrangement of the coal, and generation of**  
376 **gaseous products as described previously by Solomon et al. (1988) as well as Behar and**  
377 **Hatcher (1995). First, a large amount of CO<sub>2</sub> is generated; then, gaseous hydrocarbons**  
378 **are produced in lower amounts. As much CO<sub>2</sub> (5.8% of carbon) is released by**  
379 **defunctionalisation as is generated as gaseous and liquid hydrocarbons (4.8% totally as**  
380 **methane, butane and C<sub>14+</sub> liquid hydrocarbons). NMR data confirm that CO<sub>2</sub> is formed**  
381 **by defunctionalisation of carboxyl and carbonyl functional groups. The methane**  
382 **generated is insufficient to be associated with the loss of methoxy groups in NMR**  
383 **spectra (5.3% of carbons). At low maturation levels, methyl radicals, presumably**

384 derived from removal of methoxy groups, may be involved in multiple reaction  
385 pathways forming various pyrolytic products as well as solid, liquid or gaseous  
386 hydrocarbons. Alternatively, methoxy groups may form methanol or formaldehyde,  
387 both of which could not be measured directly in this study. Methane and butane could  
388 derive from reactions of methyl radicals but they also could evolve from pyrolytic  
389 degradation of the aliphatic side chains in lignin. This process could involve  
390 defunctionalisation of the side chain followed by pyrolysis.

391 Thermal evolution of the insoluble portion of the coal leads to an increase in cross  
392 linking and in the presence of symmetric aromatic structures. This process is in  
393 complete agreement with the cross-link processes at low temperature proposed by  
394 Solomon et al. (1990) who suggested that, at low temperature and prior to tar evolution,  
395 cross linking of the kerogen is correlated to CO<sub>2</sub> loss, water and light hydrocarbons  
396 generation. We determined by quantitative NMR that half of the side chains  
397 disappeared by formation of gaseous products (CO<sub>2</sub>, methane and butane).

398 Behar and Hatcher (1995) have shown that the liquid C<sub>14+</sub> fraction contains  
399 aromatic structural units. However, these are minor as our carbon balance indicates  
400 that they represent only 1.1% of the carbon. This suggests that aromatic rings in the  
401 residue are not significantly lost. Characterization by HRMAS NMR of the mature  
402 sample shows that linkages between the aromatic rings and the aliphatic side chains  
403 increase but do not enhance the aromaticity of the structure. Oxygenated and  
404 protonated carbons on the aromatic rings are converted to carbon-carbon linkages and  
405 the proportion of CH increases in the side chains. The proportion of naphthenic rings  
406 seems to increase upon maturation, perhaps because of the alteration of the linear side  
407 chains.

408

## 409 6. Conclusions

410 This paper is part of a study that seeks to define the relative importance of  
411 defunctionalisation and cracking processes during early thermal decomposition of fossil  
412 organic matter from numerous sources. Understanding and quantifying those processes is  
413 paramount to developing improved kinetic models that are used to evaluate the extent of  
414 petroleum generation in sedimentary basins. This paper examines the early reactions for the  
415 thermal evolution of a Type III kerogen using as a starting point the chemistry of a sample  
416 derived from coalified wood collected from the Gippsland Formation, Morwell open cut mine  
417 in Victoria, Australia. The experimental data obtained from artificial maturation in a closed-  
418 system reactor will be used for comparison with results of a joint study that proposes use of a  
419 new technique for determining maturation changes, that of molecular dynamics simulations  
420 with a reactive force field. The structural model for the Morwell coal proposed in this paper  
421 (Figure 4) is the only input data of the molecular dynamics simulations. For this reason, the  
422 lignin model of Nimz, (1974) is selected to represent the angiospermous origin of the  
423 Morwell sample.

424 All the structural changes mentioned in this paper lead to a rearrangement of the coal  
425 that can be described through a molecular model that is the subject of a future paper. We  
426 expect in this future study to reproduce by molecular dynamic simulations the chemical  
427 processes experimentally observed in the current paper in order to validate the simulation  
428 procedure and to confirm, from a theoretical point of view, reactions processes proposed here  
429 and in the literature. In a way, positive results from the dynamic simulations will also validate  
430 the structural model for the Morwell coal.

431

432

433

434

## Acknowledgements

435 The experimental facilities used for this research were provided by the IFP (Institut Français  
436 du pétrole), and the College of Sciences Major Instrumentation Cluster in Old Dominion  
437 University. Fellowship support was provided by the ANRT (Association Nationale de la  
438 Recherche Technique), CIFRE grant #458/2004.

439 The authors would like to thank Isaiah Ruhl for assistance with the NMR experiments. We  
440 also thank Neal Gupta (Department of EAPS- MIT) and anonymous reviewer for their  
441 constructive review of this manuscript.

442

## References

443 Adler, E., 1977. Lignin chemistry- Past, present and future. *Wood Science and Technology*.  
444 11, 169-218.

445 Albrecht, P., Ourisson, G., 1969. Triterpene alcohol isolation from oil shale. *Science*, 166,  
446 1192-1193.

447 Al Darouich, T., Behar, F., Largeau, C., 2006. Thermal cracking of the light aromatic fraction  
448 of Safaniya crude oil - Experimental study and compositional modeling of molecular classes.  
449 *Organic Geochemistry* 37, 1130-1154.

450 Bates, A. L., Hatcher, P. G., 1989. Solid-state <sup>13</sup>C NMR studies of a large fossil gymnosperm  
451 from the Yallourn Open Cut, Latrobe Valley, Australia. *Organic geochemistry*.14, 6, 609-617.

452 Behar, F., Hatcher, P.G., 1995. Artificial Coalification of a fossil wood from Brown Coal by  
453 confined system pyrolysis. *Energy & Fuels* 9, 984-994.

454 Behar, F., Leblond, C., Saint-Paul, C., 1989. Analyse quantitative des effluents de pyrolyse en  
455 milieu ouvert et fermé. *Oil and Gas Science and Technology* 44, 387-411.

456 Dria, K. J., Sachleben, J. R., Hatcher, P. G., 2002. Solid-state carbon-13 nuclear magnetic  
457 resonance of humic acids at high magnetic field strengths. *Journal of Environmental Quality*,  
458 31, 393-401.

459 Fowler, M. G.; Gentzis, T.; Goodarzi, F.; Foscolos, A. E., 1991. The petroleum potential of  
460 some Tertiary lignites from northern Greece as determined using pyrolysis and organic  
461 petrological techniques. *Organic Geochemistry*, 17, 805-826.

462 Hatcher P. G., Lerch III, H. E., Bates, A. L., Verheyen, T.V., 1989. Solid-state <sup>13</sup>C nuclear  
463 magnetic resonance studies of coalified gymnosperm xylem tissue from Australian brown  
464 coals. *Organic Geochemistry*.14, 2, 145-155.

465 **Hatcher, P.G., 1988. Dipolar-Dephasing <sup>13</sup>C NMR Studies of Decomposed Wood Structure  
466 and Changes Associated with Defunctionalization of Lignin Structural Units during  
467 Coalification and Coalified Xylem Tissue: Evidence for Chemical. *Energy & Fuel*, 48-58.**

468 Hatcher, P. G., 1989. Chemical structure models for coalified wood (vitrinite) in low rank  
469 coal. *Organic Geochemistry* 16, 959-968.

- 470 Hatcher, P. G., Clifford, D. J., 1997. The organic geochemistry of coal: from plant materials to  
471 coal. *Organic Geochemistry* 27, 251-274.
- 472 Hatcher, P.G., Wilson, M.A., Vassallo, A.M., Lerche III, H. E., 1989. Studies of  
473 angiospermous wood in Australian brown coal by nuclear magnetic resonance and analytical  
474 pyrolysis: new insights into the early coalification process. *International Journal of Coal*  
475 *Geology* 13, 99-126.
- 476 Holdgate, G. R., 1985. Latrobe Valley Brown Coals\_ Their geometry and facies equivalents as  
477 a guide to depositional environment. *Australian Coal Geology* 5, 53-68.
- 478 Louis M., Tissot B., 1967. Influence de la température et de la pression sur la formation des  
479 hydrocarbures dans les argiles à kérogène. 7th World Petroleum Congress, Mexico, 2, 47-60.
- 480 Mukhopadhyay, P. K., Hatcher, P., Calder, J. H., 1991. Hydrocarbon generation from deltaic  
481 and intermontane fluviodeltaic coal and coaly shale from the Tertiary of Texas and  
482 Carboniferous of Nova Scotia. *Organic Geochemistry* 17, 765-783.
- 483 Mc Kinney, D. E., Hatcher, P.G., 1996. Characterization of peatified and coalified wood by  
484 tetramethylammonium hydroxide (TMAH) thermochemolysis. *International Journal of Coal*  
485 *Geology* 32, 217-228.
- 486 Nelson, C. R., Li, W., Lazar, I. M., Larson, K. H., Malik, A., Lee, M. L., 1998. Geochemical  
487 Significance of n-Alkane Compositional-Trait Variations in Coals. *Energy & Fuels* 12, 277-  
488 283.
- 489 Nimz, H., 1974. Beech lignin-proposal of a constitutional scheme. *Angewandte Chemie*  
490 *International Edition*, England 74, 313\_321
- 491 Payne, D. F., Ortoleva, P. J., 2002. A model for lignin alteration—part I: a kinetic reaction-  
492 network model. *Organic Geochemistry* 32, 1073-1085.
- 493 Philippi, G.T., 1965. On the depth, time and mechanism of petroleum generation. *Geochimica*  
494 *and Cosmochimica Acta* 29, 1021-1049.
- 495 Philp, R. F., Gilbert, T. D., and Russell, N. J., 1982. Characterization of Victoria brown coals  
496 by pyrolysis techniques combined with gas chromatography and gas chromatography-mass  
497 spectrometry. *Australian Coal Geology* 4, 228-243.
- 498 Rappé, A.K., Casewit, C.J., Colwell, K.S., Goddard III, W.A. and Skid, W.M., 1992. UFF, a  
499 full periodic table force field for molecular mechanics and molecular dynamics simulations.  
500 *Journal of American Chemical Society*, 114, 10024-10039.
- 501 Root, D.M., Landis, C.R. and Cleveland, T., 1993. Valence Bond Concepts Applied to the  
502 molecular mechanics description of molecular Shapes. 1. Application to nonhypervalent  
503 molecules of the P-block. *Journal of American Chemical Society* 115, 4201-4209.
- 504 Root, D.M., 1997. Ph.D. thesis, University of Wisconsin, Madison, USA.
- 505 Salmon, E., Behar, F., Lorant, F., Hatcher, P.G., Metzger, P., Marquaire, P-M., 2008 accepted  
506 manuscript. Thermal decomposition process in algaenan of *Brotryococcus braunii* race L.  
507 Part1: Experimental data and structural evolution. *Organic Geochemistry*, *accepted*  
508 *manuscript*.
- 509 Solomon P.R., Hamblen D.G., Carangelo R.M., Serio M.A., Deshpande G.V., 1988. General  
510 model of coal devolatilization. *Energy and Fuels*, 2, 405-422.
- 511 Solomon, P. R., Serio, M.A., Deshpande, G.V., Kroo, E., 1990. Cross-linking reactions during  
512 coal conversion. *Energy & Fuels* 4, 42-54.

- 513 Spackman, W., Barghoorn, E.S., 1966. Coalification of woody tissue as deduced from a  
514 petrographic study of Brandon lignite. *Coal Science. American Chemical Society Adv.* 55,  
515 695-707.
- 516 Stout, S. A., Boon, J. J., Spackman, W., 1988. Molecular aspects of peatification and early  
517 coalification of angiosperm and gymnosperm wood. *Geochimica. Cosmechimica Acta* 52,  
518 405-414.
- 519

520 **Table captions**

521

522 **Table 1.** Comparison of the structural composition of the Morwell sample (Behar and Hatcher  
523 1995) with that of the brown coal model of Hatcher (**1989**).

524

525 **Table 2.** Structural composition of the fresh lignin model (Nimz, 1974) and of the model and  
526 sample of the Morwell coalified wood.

527

528 **Table 3.** Mass and atomic balances of the experimental thermal decomposition of the  
529 Morwell coal.

530

531 **Figure captions**

532

533 **Figure 1.** (a) Brown coal molecular model from Hatcher (1990). (b) Typical units in lignin :  
534 numbering convention

535 **Figure 2.** Early diagenesis reactions selected to transform the lignin structure to mature rank  
536 of lignite. (Hatcher, 1989; Hatcher and Clifford, 1997; Payne and Ortoleva, 2002)

537 **Figure 3.** Beech lignin model from Nimz (1974)

538 **Figure 4.** Structural model of the Morwell sample at coal rank of lignite.

539 **Figure 5.** DPMAS  $^{13}\text{C}$  NMR data of the initial sample of Morwell lignite (A ) and residue (B)  
540 recovered after thermal stress (300°C/9h). The inset table provides quantitative measurements  
541 of the relative contributions of the various carbons. The % loss of carbon during artificial  
542 maturation is also indicated. The errors ( $\pm$ ) are given for each calculated value and represent a  
543 relative error of 3% for peak area measurements.

544 **Figure 6.** FTIR spectra of the initial sample of Morwell lignite (A) and the residue (B)  
545 recovered after thermal stress (300 °C/9 h). Various assignments for stretching ( $\nu$ ) and  
546 deformation ( $\delta$ ) frequencies.

547 **Figure 7.** HSQC spectra of the initial sample of Morwell lignite and the residue recovered after  
548 thermal stress (300 °C/9 h). Boxed out regions are discussed in the text. The solvent peak is for  
549 DMSO. The left ordinate projection is the respective DPMAS  $^{13}\text{C}$  NMR spectrum.

550 **Figure 8.** Extended aliphatic region of the HSQC NMR spectra in Figure 9 of the initial  
551 Morwell lignite and the residue recovered at 300°C/9 h. Structural assignments for the indicated  
552 carbon are presented in a table below of the spectra.

553 **Figure 9.** TOCSY spectra of the initial Morwell lignite and the residue recovered at 300°C/9  
554 h. Structural assignments for some cross peaks are listed in Figure 8. Boxed out regions are  
555 discussed in the text. The solvent peak is for DMSO.

556  
557 **Figure 10.** Expanded view of the TOCSY spectrum in Figure 9. Structural assignments for the  
558  $^1\text{H}$ s are presented in a table below of the data with chemical shifts indicated for each coupled  
559 system.

560  
561 **Figure 11.** Carbon mass balance of the Morwell lignite sample during 300°C/9h closed pyrolysis.

562

563 **Table 1.** Comparison of the structural composition of the Morwell sample (Behar and Hatcher  
 564 1995) with that of the brown coal model of Hatcher (1989).

chemical type	Morwell Sample (Behar et al. 1995)	Brown coal Model (Hatcher 1989)
atomic C (%)		
C=O	2.90	2.78
COOH	4.00	1.85
C <sub>aro</sub> -OR <sub>1</sub>	22.80	21.30
C <sub>aro</sub> -	39.50	45.37
O-CH <sub>3</sub>	3.10	4.63
C-O-R <sub>2</sub>	4.00	5.56
-CH, -CH <sub>2</sub> , -CH <sub>3</sub>	23.10	18.52
total	99.40	100.01
<i>f<sub>a</sub></i>	62.30	66.67
formula	-	C <sub>108</sub> H <sub>102</sub> O <sub>34</sub>
H/C	0.89	0.94
O/C	0.33	0.31

*f<sub>a</sub>*: aromaticity, R<sub>1</sub> : H or -CH<sub>3</sub>, R<sub>2</sub>: H, -C-

565

566

567

568

569 **Table 2.** Structural composition of the fresh lignin model (Nimz, 1974) and of the model and  
 570 sample of the Morwell coalified wood.

chemical structure	Lignin Model	Morwell Model	Morwell Sample
	% C	% C	% C
-C=O	3.1	3.0	3.5
-COOH	0.4	6.4	6.6
-Caro-OR <sub>1</sub>	22.8	24.4	25.8
=Caro-	35.1	39.7	39.1
-C-O-R <sub>2</sub>	18.9	3.0	2.1
-O-CH <sub>3</sub>	13.1	6.0	6.1
-CH, -CH <sub>2</sub> , -CH <sub>3</sub>	6.6	17.5	16.9
total	100.0	100.0	100.0
<i>fa</i>	57.9	64.1	64.9
Formula	C <sub>259</sub> H <sub>306</sub> O <sub>93</sub>	C <sub>234</sub> H <sub>216</sub> O <sub>96</sub>	
H/C	1.18	0.92	0.94
O/C	0.359	0.410	0.390

*fa*: aromaticity, R<sub>1</sub> : H or -CH<sub>3</sub>, R<sub>2</sub>: H, -C-

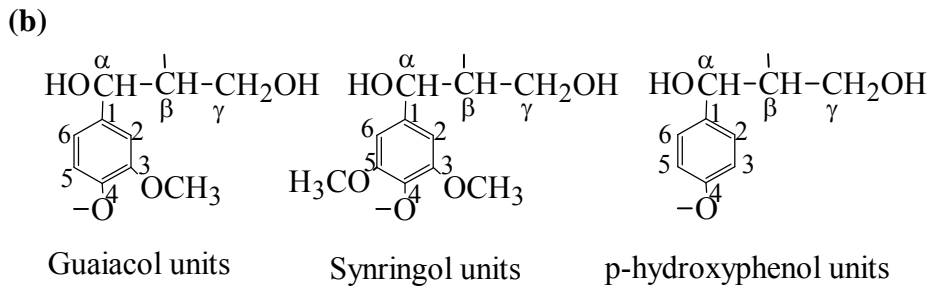
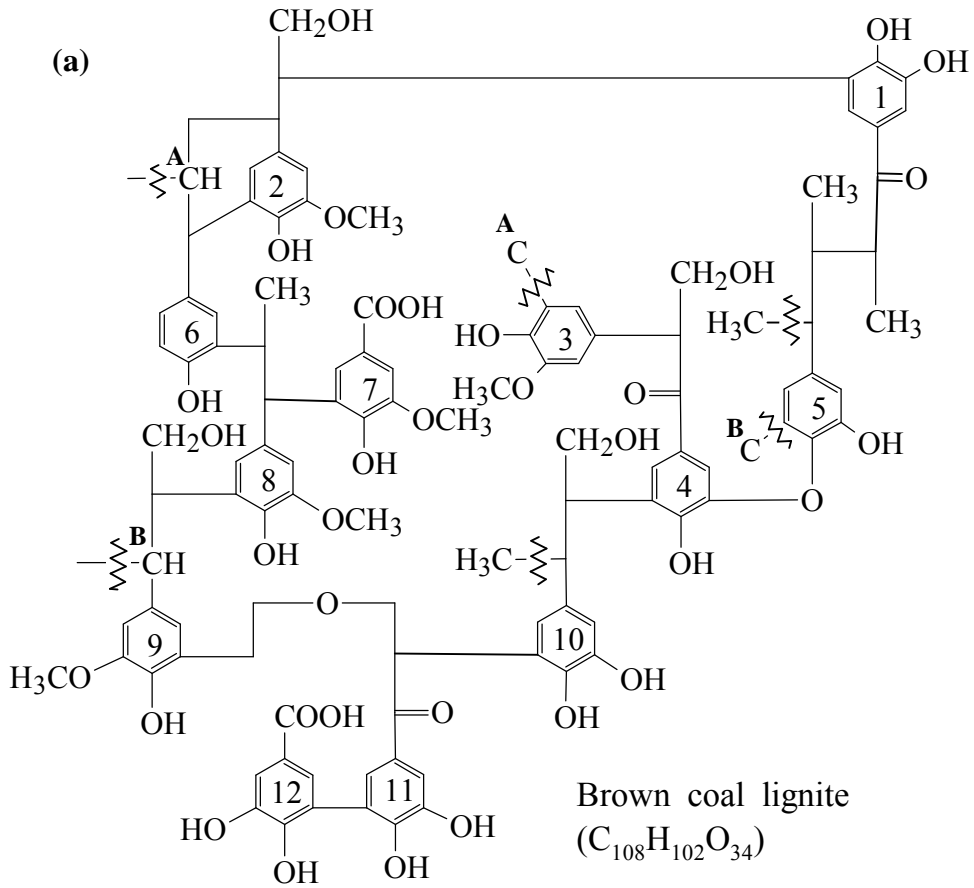
571  
572  
573  
574  
575  
576  
577  
578

**Table 3.** Mass and atomic balances of the experimental thermal decomposition of the Morwell coal.

T	t	CO <sub>2</sub>	CH <sub>4</sub>	C <sub>4</sub>	C <sub>7</sub> -C <sub>14</sub>	C <sub>14</sub> +			Residue		
						n-C <sub>5</sub>	DCM	Total	yield	H/C	O/C
°C	h	mg/g							mg/g	atomic ratio	
initial										0.94	0.39
200	9	45.8	<0.1	2.5	<0.1	1.3	2.6	52.2	947.8	0.88	0.34
225	9	66.5	<0.1	4.6	<0.1	1.4	4.0	76.5	923.5	0.86	0.31
250	9	93.2	0.1	5.5	<0.1	1.4	6.5	106.7	893.3	0.80	0.29
275	9	105.7	0.4	8.7	<0.1	1.4	6.2	122.4	877.6	0.73	0.26
300	9	129.9	1.1	26.5	<0.1	1.7	7.2	166.4	833.6	0.69	0.22

579  
580  
581

582 **Figure 1.** (a) Brown coal molecular model from Hatcher (1990). (b) Typical units in lignin :  
 583 numbering convention



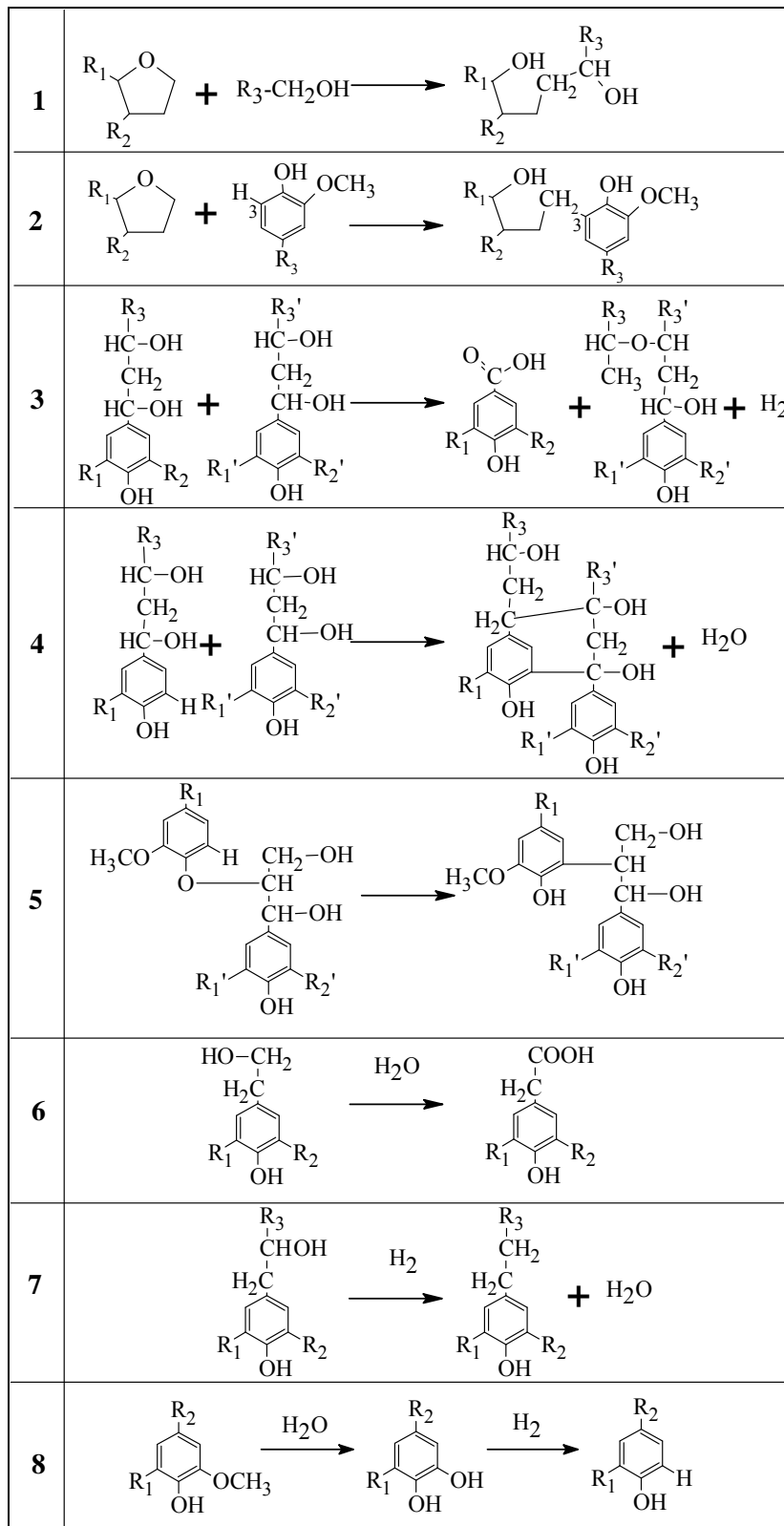
584

585

586

587 **Figure 2.** Early diagenesis reactions selected to transform the lignin structure to mature rank

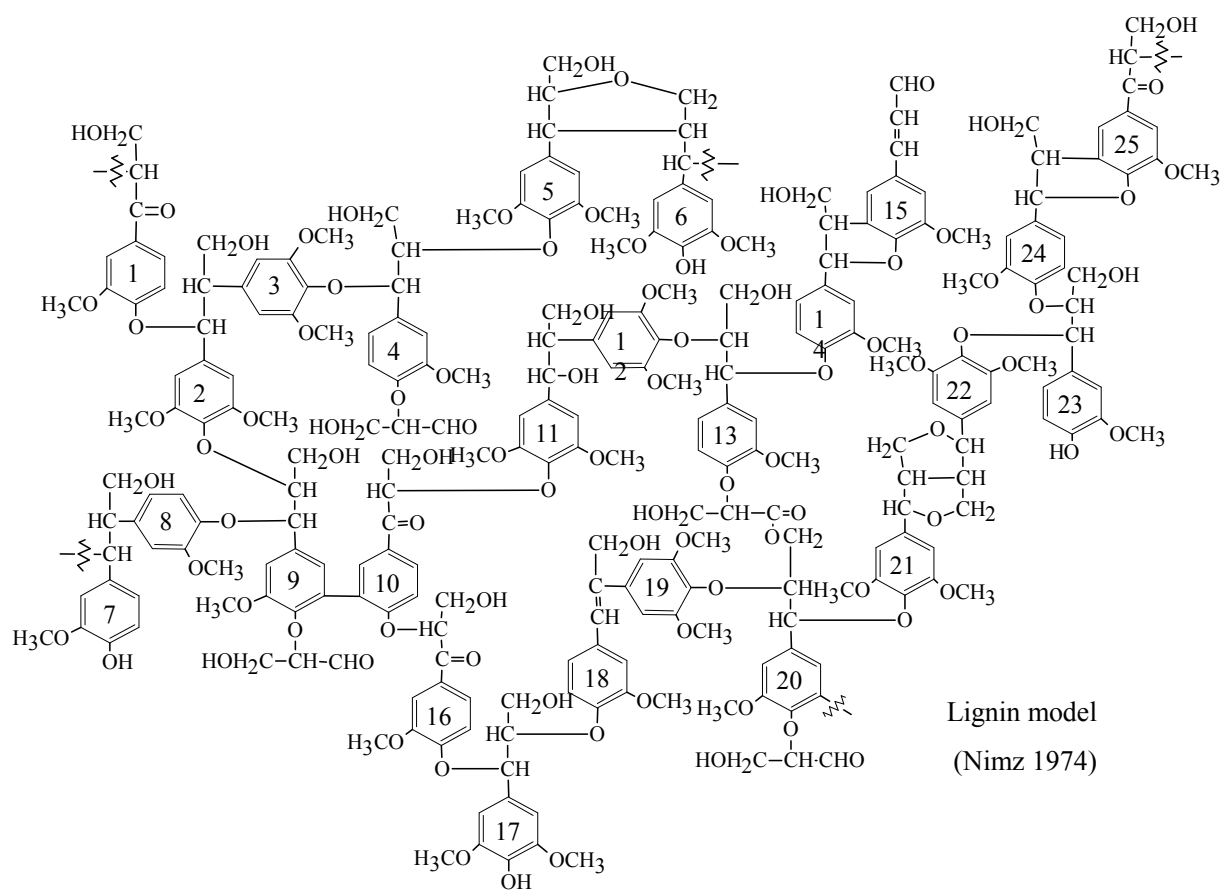
588 of lignite. (Hatcher, 1989; Hatcher and Clifford, 1997; Payne and Ortoleva, 2002)



589

590

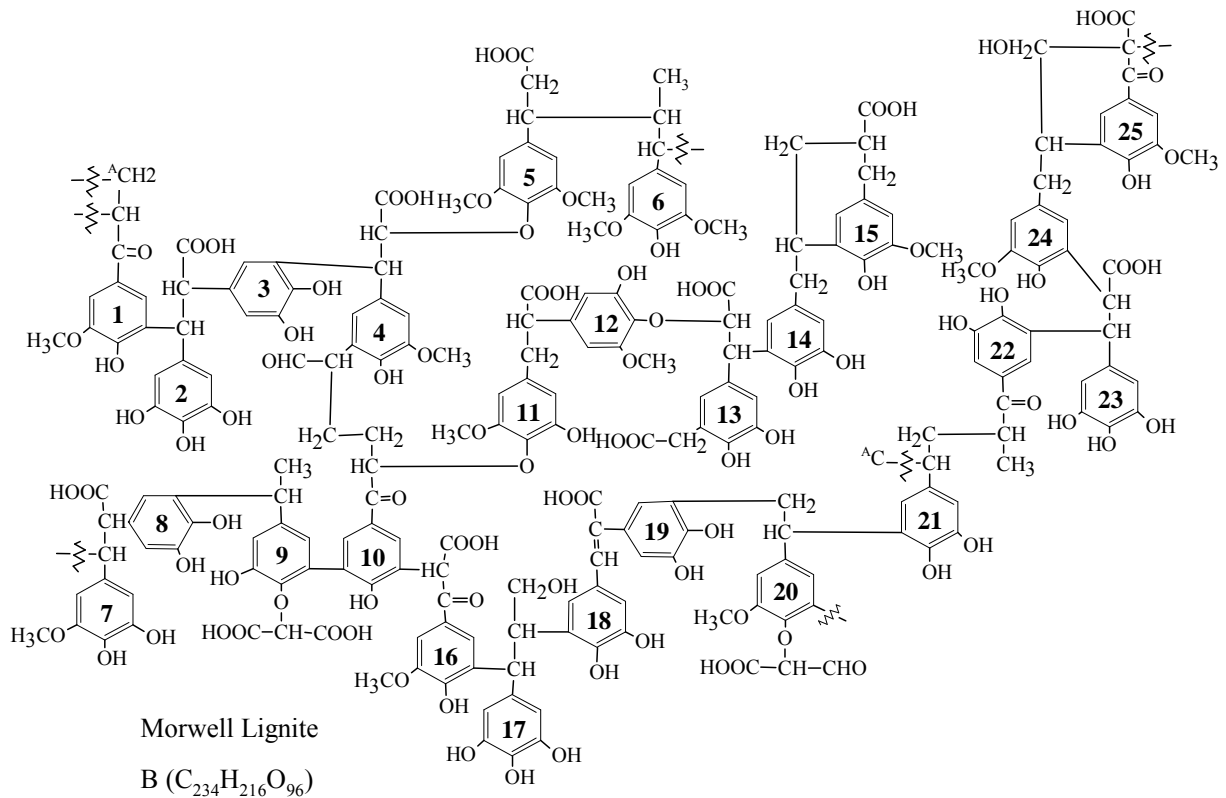
591 **Figure 3.** Beech lignin model from Nimz (1974)



592

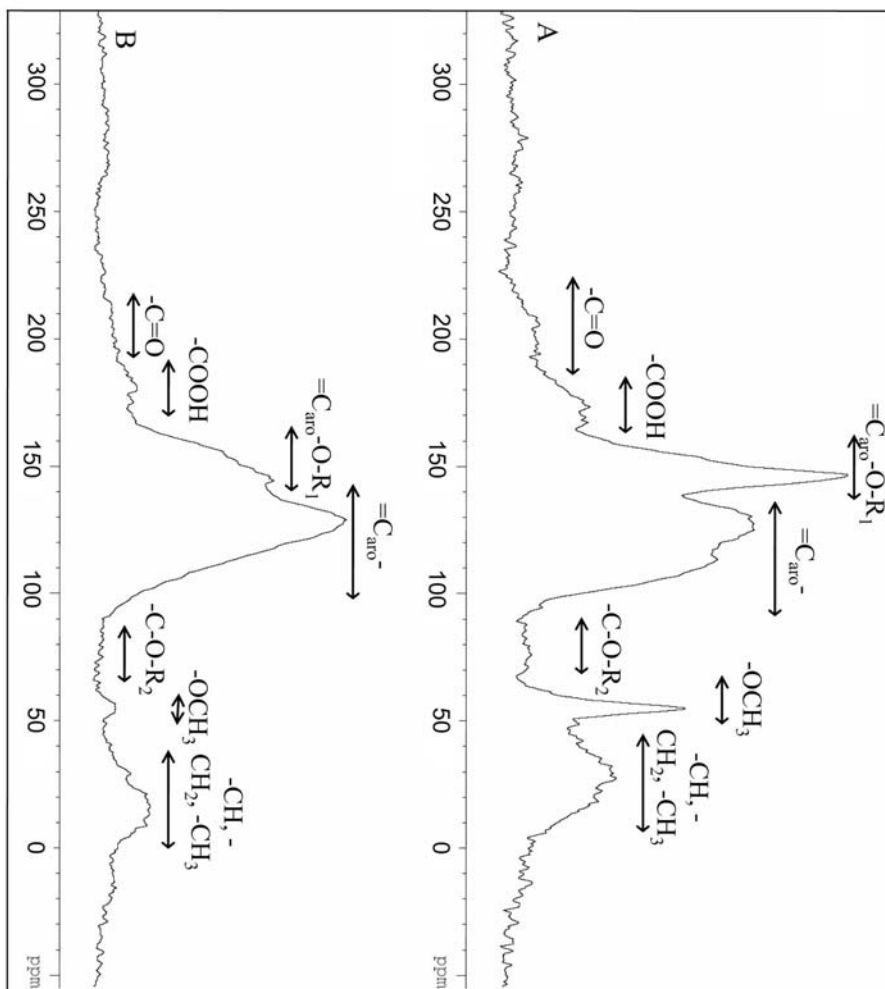
593

594 **Figure 4.** Structural model of the Morwell sample at coal rank of lignite.



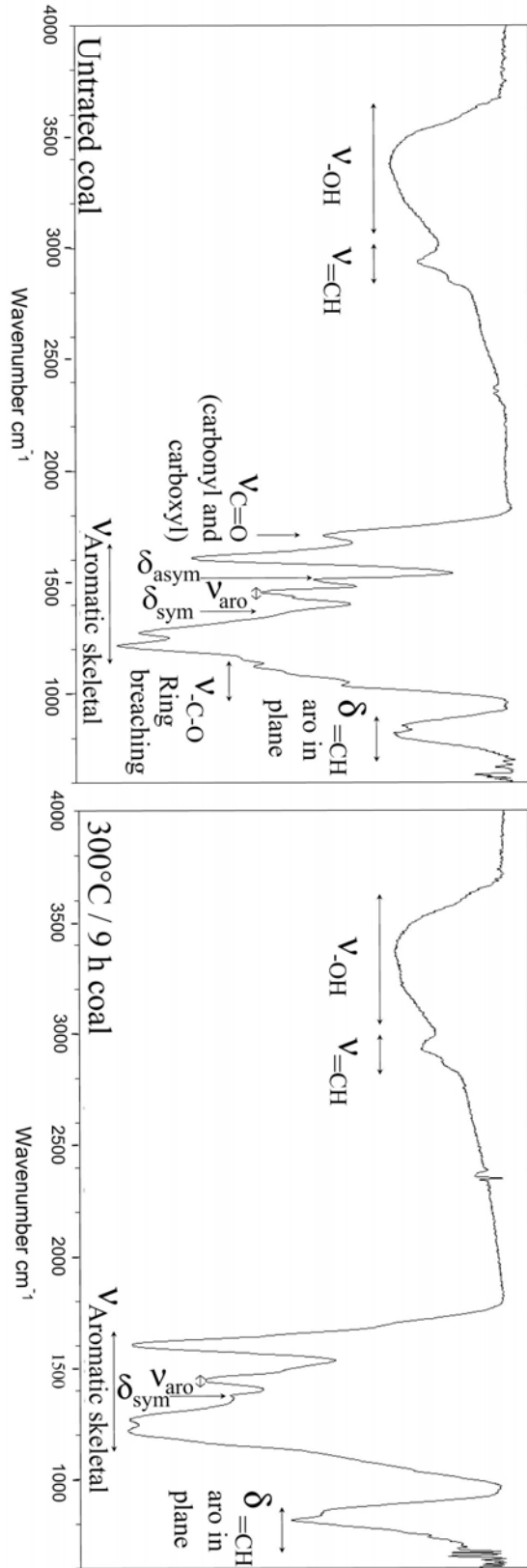
595

596 **Figure 5.** DPMAS  $^{13}\text{C}$  NMR data of the initial sample of Morwell lignite (A) and residue (B)  
 597 recovered after thermal stress (300 °C/9 h). The inset table provides quantitative  
 598 measurements of the relative contributions of the various carbons. The % loss of carbon  
 599 during artificial maturation is also indicated. The errors ( $\pm$ ) are given for each calculated value  
 600 and represent a relative error of 3% for peak area measurements.



chemical type	Initial sample Carbon (atomic %)	300°C 9h	total C loss %
-C=O	3.5 ± 0.1	2.9 ± 0.1	-0.6
-COOH	6.6 ± 0.2	3.7 ± 0.1	-2.9
=Caro-O-R <sub>1</sub>	25.8 ± 0.8	19.2 ± 0.6	-6.5
=Caro-	39.1 ± 1.2	47.7 ± 1.4	8.6
-C-O-R <sub>2</sub>	2.1 ± 0.06	0.4 ± 0.01	-1.7
-O-CH <sub>3</sub>	6.1 ± 0.2	0.8 ± 0.02	-5.3
-CH <sub>1</sub> , -CH <sub>2</sub> , -CH <sub>3</sub>	16.9 ± 0.5	8.7 ± 0.3	-8.2
total	100.0	83.4	-16.6
<i>fa</i>	64.9 ± 2	66.9 ± 2	2.1
% (=Caro-O-R <sub>1</sub> )	39.8%	28.8%	-11.0%
% (=Caro-)	60.2%	71.2%	11.0%
all/aro	0.26	0.13	

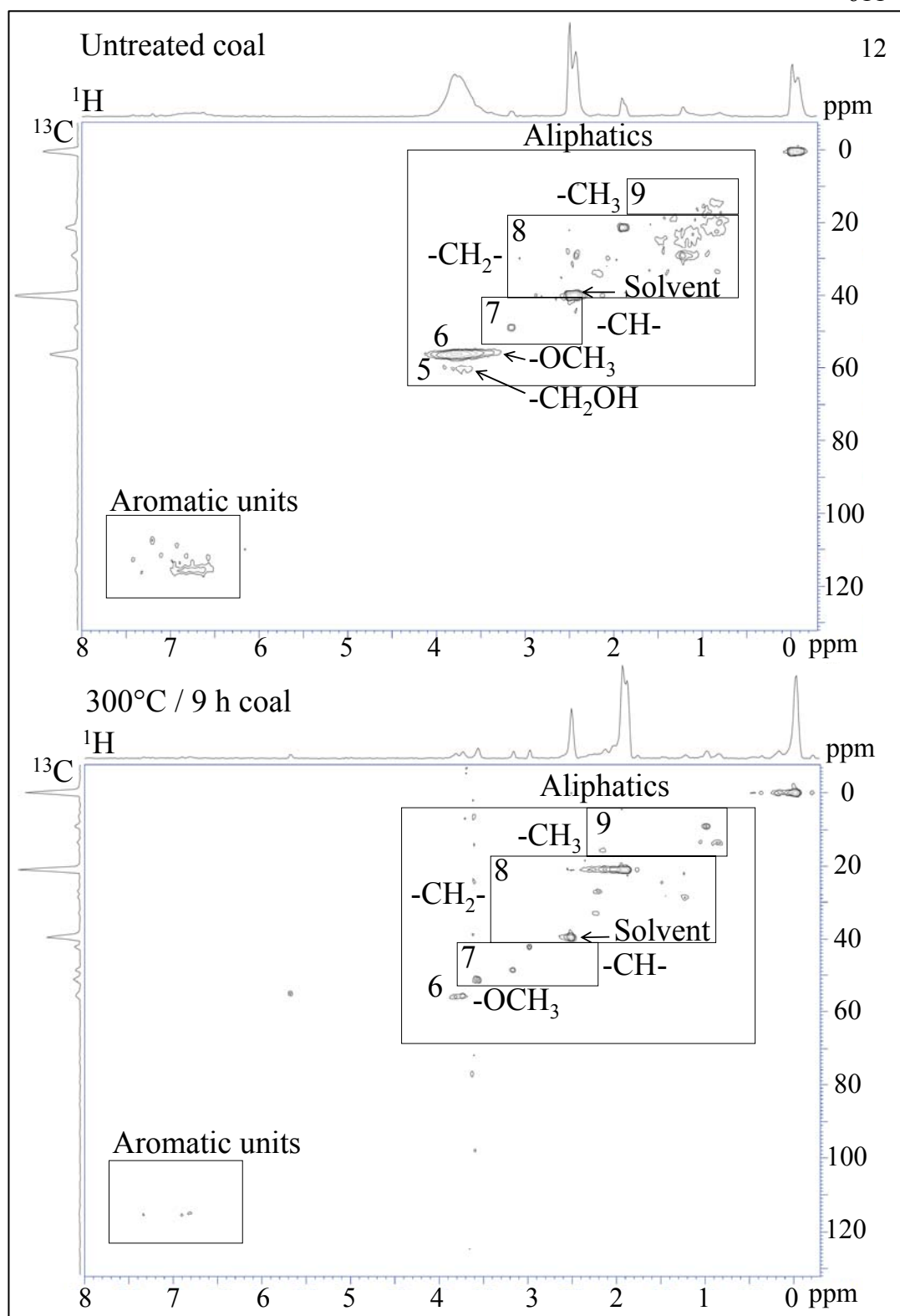
603 **Figure 6.** FTIR spectra of the initial sample of Morwell lignite (A) and the residue (B)  
 604 recovered after thermal stress (300°C/9h). Various assignments for stretching ( $\nu$ ) and  
 605 deformation ( $\delta$ ) frequencies.



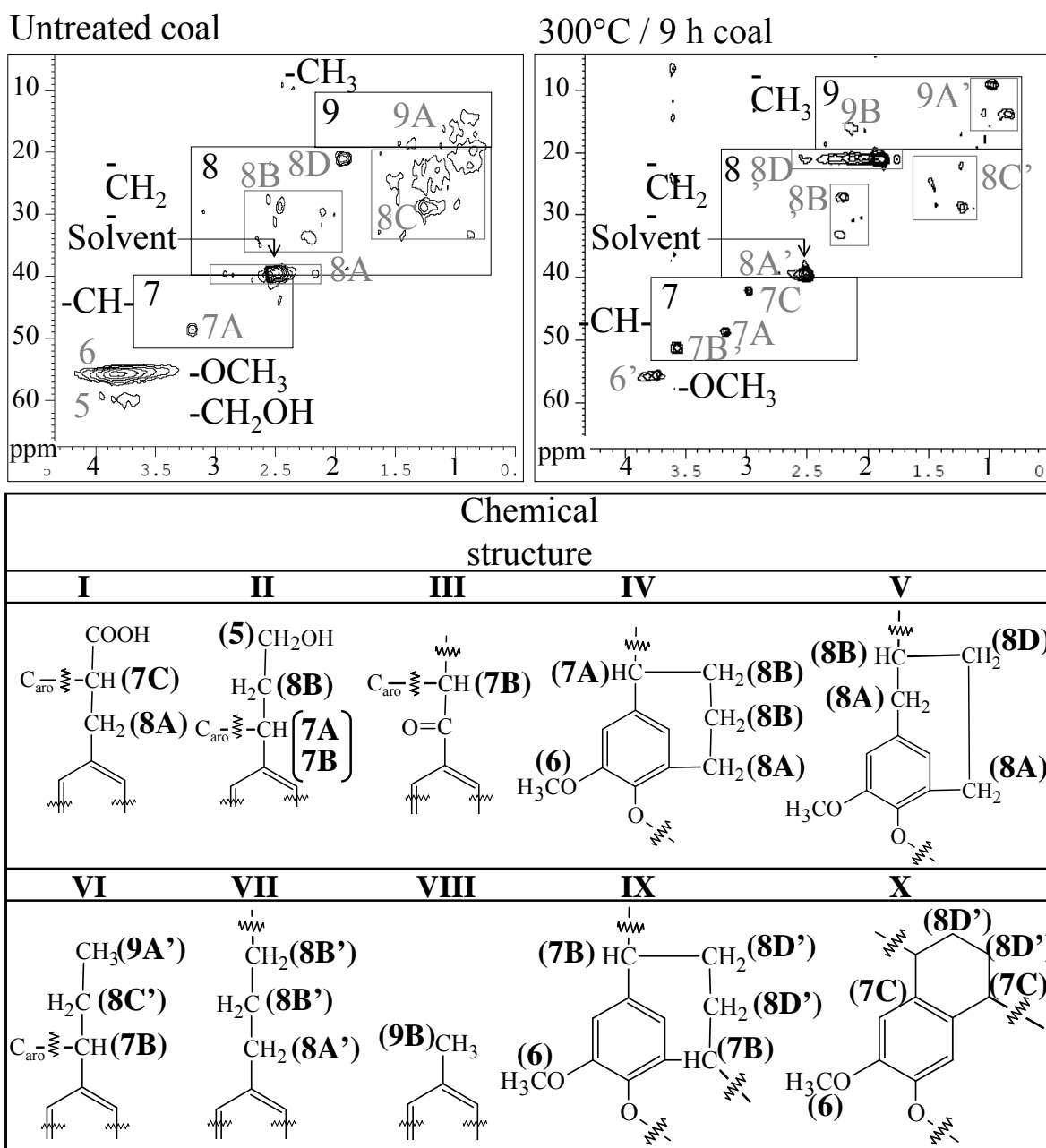
606  
 607

608 **Figure 7.** HSQC spectra of the initial sample of Morwell lignite and the residue recovered after  
609 thermal stress (300 °C/9 h). Boxed out regions are discussed in the text. The solvent peak is for  
610 DMSO. The left ordinate projection is the respective DPMAS  $^{13}\text{C}$  NMR spectrum.

611

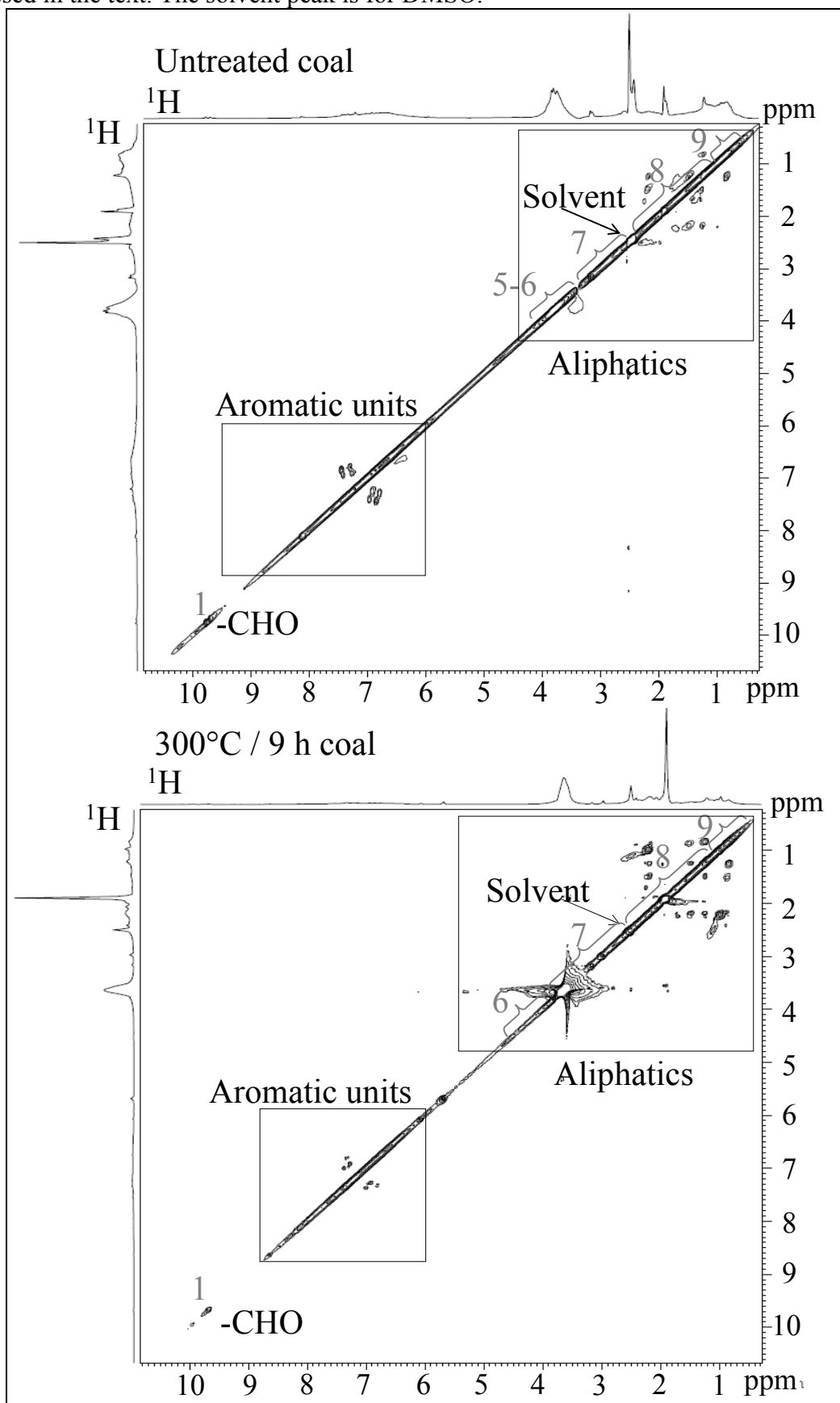


613 **Figure 8.** Extended aliphatic region of the HSQC NMR spectra in Figure 9 of the initial  
 614 Morwell lignite and the residue recovered at 300°C/9 h. Structural assignments for the indicated  
 615 carbon are presented in a table below of the spectra.

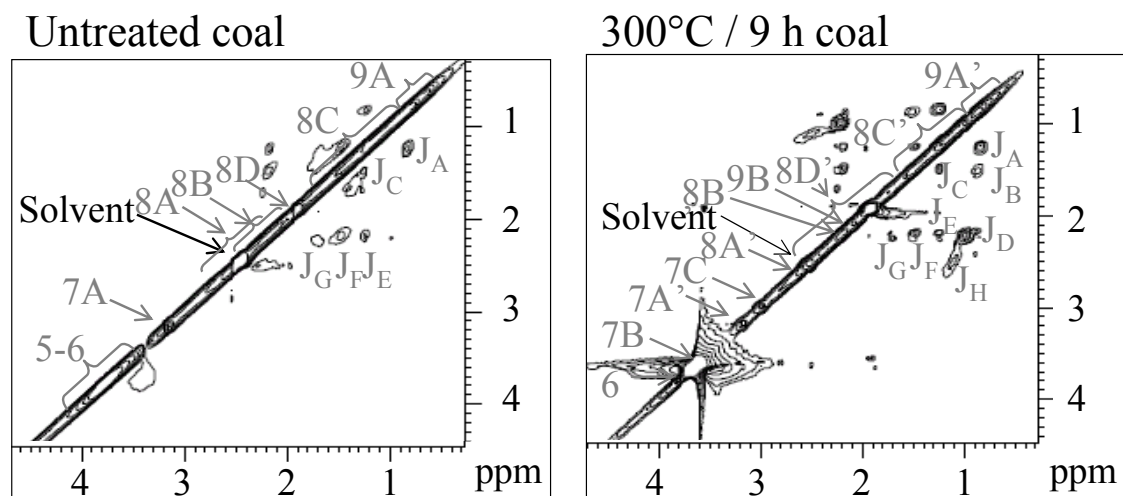


616

617 **Figure 9.** TOCSY spectra of the initial Morwell lignite and the residue recovered at 300°C/9  
618 h. Structural assignments for some cross peaks are listed in Figure 8. Boxed out regions are  
619 discussed in the text. The solvent peak is for DMSO.



621 **Figure 10:** Expanded view of the TOCSY spectrum in Figure 9. Structural assignments for the  
 622  $^1\text{H}$ s are presented in a table below of the data with chemical shifts indicated for each coupled  
 623 system.



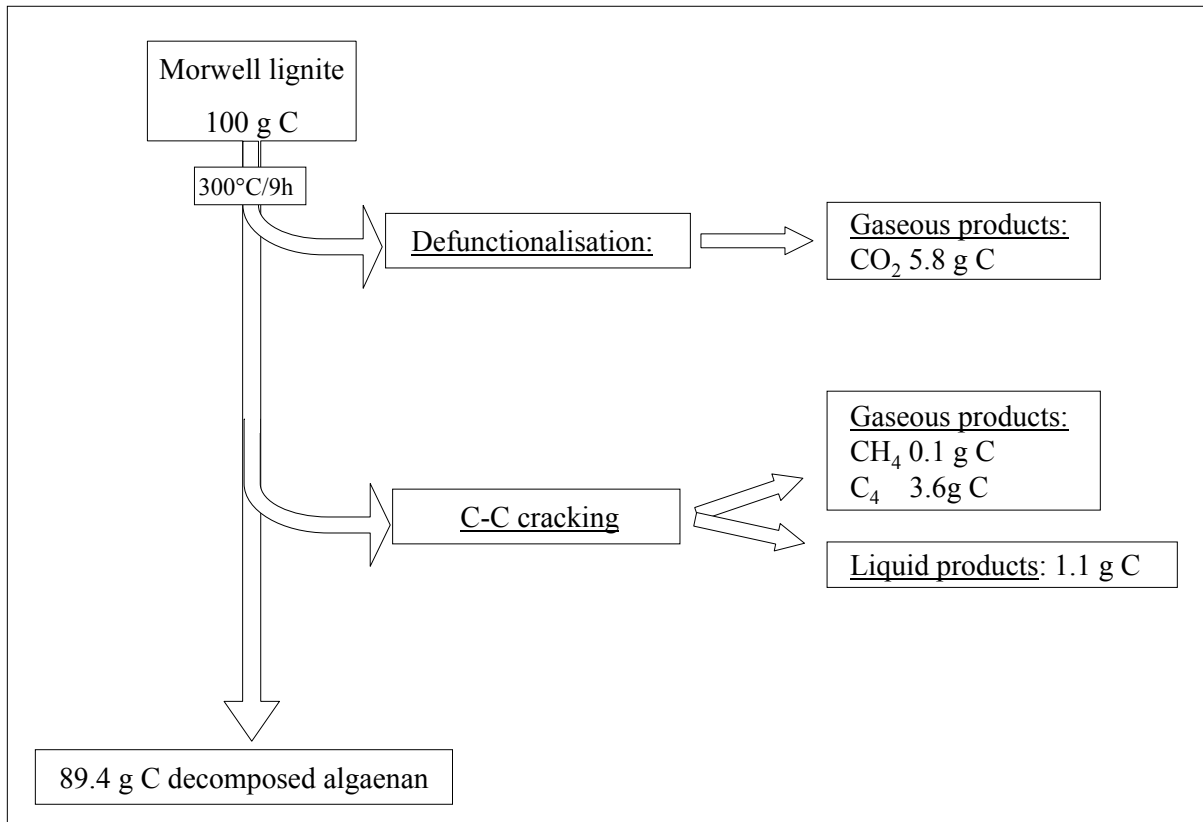
Chemical structure	Assignment coupling	Assignment carbons	$\delta^1\text{H}$	
			$\text{H}_x$	$\text{H}_y$
			ppm	
$\begin{array}{c} \text{CH}_3 \mathbf{a}_0 \\   \\ \text{CH}_2 \mathbf{a}_1 \\   \\ \text{H}_2\text{C} \mathbf{a}_2 \\   \\ \text{CH}_2 \mathbf{a}_3 \\   \\ \text{C}=\text{C} \end{array}$	$J_A$	$\mathbf{a}_0\text{-a}_1, \mathbf{b}_0\text{-b}_1, \mathbf{d}_0\text{-d}_2$	0.8	1.3
$\begin{array}{c} \text{CH}_3 \mathbf{b}_0 \\   \\ \text{H}_2\text{C} \mathbf{b}_1 \\   \\ \text{CH}_2 \mathbf{b}_2 \\   \\ \text{C}=\text{C} \end{array}$	$J_B$	$\mathbf{a}_0\text{-a}_2, \mathbf{b}_0\text{-b}_2, \mathbf{d}_0\text{-d}_1$	0.8	1.5
$\begin{array}{c} \text{C}=\text{C} \\   \quad   \\ \text{CH}_2 \mathbf{a}_1 \quad \text{CH}_2 \mathbf{a}_2 \end{array}$	$J_C$	$\mathbf{a}_1\text{-a}_2, \mathbf{b}_1\text{-b}_2, \mathbf{d}_1\text{-d}_2$	1.2	1.5
$\begin{array}{c} \mathbf{d}_0 \text{ CH}_3 \\   \\ \mathbf{d}_1 \text{ HC} \text{---} \text{CH}_2 \mathbf{d}_2 \\   \\ \mathbf{d}_2' \text{ CH}_2 \end{array}$	$J_D$	$\mathbf{d}_0\text{-d}_2'$	1.0	2.2
$\begin{array}{c} \text{CH}_3 \mathbf{c}_0 \\   \\ \text{CH}_2 \mathbf{c}_1 \\   \\ \text{C}=\text{C} \end{array}$	$J_E$	$\mathbf{a}_1\text{-a}_3, \mathbf{b}_0\text{-b}_2$	1.2	2.2
$\begin{array}{c} \text{H}_3\text{CO} \\   \\ \text{C}_6\text{H}_4 \\   \\ \text{O} \\   \\ \text{CH}_2 \mathbf{d}_3 \end{array}$	$J_F$	$\mathbf{d}_2\text{-d}_3, \mathbf{d}_2\text{-d}_2'$	1.5	2.2
	$J_G$	$\mathbf{d}_1\text{-d}_2', \mathbf{d}_1\text{-d}_3$	1.7	2.2
	$J_H$	$\mathbf{c}_0\text{-c}_1$	1.1	2.6

624

625

626

627 **Figure 11.** Carbon mass balance of the Morwell lignite sample during 300°C/9h closed pyrolysis.



628